Characterization of polyethylene films drawn by machine direction orientation and consequences on their photooxidation

Julien Christmann, Christine Taviot-Guého, Emma Mazeau, Jean-Luc Gardette, Gérard Pichon, Bruno Bouchut, Sandrine Therias

Polymer xxx (xxxx) 127692

Contents lists available at ScienceDirect

Polymer

journal homepage: www.elsevier.com/locate/polymer

Characterization of polyethylene films drawn by machine direction orientation and consequences on their photooxidation

Julien Christmann [a, *], Christine Taviot-Guého [a], Emma Mazeau [a], Jean-Luc Gardette [a], Gérard Pichon [b], Bruno Bouchut [b], Sandrine Therias [a, **]

[a] Université Clermont Auvergne, CNRS, Clermont Auvergne INP, ICCF, F-63000, Clermont-Ferrand, France
[b] Barbier Group, F-43600, Sainte Sigolène, France

ARTICLE INFO

Keywords:
Machine direction orientation
Photooxidation
Permeability

ABSTRACT

The effect of uniaxial drawing by Machine Direction Orientation (MDO) on polyethylene films was first studied by complementary analytical methods. XRD and polarized FTIR spectroscopy revealed the transformation of the initial spherulitic structure of PE into microfibrils composed of small crystalline blocks connected by amorphous chains oriented along the drawing direction. No stress-induced crystallization was observed upon MDO processing, but the permeability to oxygen was reduced by 30 % owing to this morphology change. In a second time, the effect of photooxidation on undrawn and MDO-drawn films was studied. There was no difference in the photooxidation kinetics and stoichiometry between them. A slight reorganization of the polymer structure due to physical ageing was observed before any photooxidation, but no change in orientation occurred upon photochemical ageing. Finally, the oxygen permeability of undrawn and MDO-drawn films decreased owing to the changes brought by photooxidation, especially the formation of polar functions within the initially apolar polyethylene and the occurrence of chemicrystallization.

1. Introduction

At the industrial scale, polyethylene (PE) can be manufactured by a huge number of processes, which contributes to its place as the world-wide most consumed polymer [1]. Among these processes, Machine Direction Orientation (MDO) consists in drawing a polymer film below its melting temperature ("cold drawing" process) to enhance several of its properties (especially mechanical, optical and barrier ones) while reducing the amount of matter necessary to reach them [2–4]. The unit used to perform this process is composed of a series of rolls subdivided into four areas corresponding to the consecutive steps of the process, *i.e.* preheating, drawing, annealing and cooling [2,4]. Preheating rolls are intended to heat uniformly the film before it is drawn between two rolls ("slow drive" SD and "fast drive" FD). Passing on heated annealing rolls enables thermal stabilization of the drawn film, especially its shrinkage ability. Final steps consist in cooling the film to room temperature on water-cooled rolls and winding. The draw ratio (DR) is finally defined as the ratio between the speeds of the last cooling roll and the first preheating roll.

It is known that, upon uniaxial drawing, the initial spherulitic morphology of semi-crystalline PE is progressively transformed into a fibrillar structure [5–10]. Several models have been proposed to explain this transformation, involving either crystallographic slips and interlamellar processes [5–7,9,11–14] or melting-crystallization [5,6,9]. According to the crystallographic model, initial lamellae are fragmented into smaller crystalline blocks by means of mechanical twinning, stress-induced martensitic phase transition and crystalline slips, associated with interlamellar processes (shear, separation and lamellae-stack rotation). Melting-crystallization involves local stress-induced melting, giving birth to new small crystalline blocks upon crystallization. As a result of both models, microfibrils oriented along the drawing direction (hereafter called the MD) are formed [15–18], which are composed of small crystalline blocks connected by amorphous chains.

A consequence of this morphology transition is the improvement of several properties of PE when compared to an undrawn sample of same thickness, *e.g.* optical properties (increased transparency and gloss, reduced haze) [19–21], mechanical properties (enhanced Young modulus along the MD and TD – Transverse Direction – and stress at break along the MD, decreased deformation at break along the MD) [19–22] and

* Corresponding author.
** Corresponding author.
E-mail addresses: julien.christmann@uca.fr (J. Christmann), sandrine.therias@uca.fr (S. Therias).

https://doi.org/10.1016/j.polymer.2024.127692
Received 9 July 2024; Received in revised form 30 September 2024; Accepted 7 October 2024
0032-3861/

barrier properties (lower permeability to oxygen and water vapour) [19,22]. However, it should be noted that, despite several decades of use at the industrial level [23], the MDO process and its consequences on the properties of PE have received little interest from a fundamental point of view [19–22,24–27], with no mention of photoageing.

Polyethylene, like all polymers, is prone to degradation under environmental stresses (heat, UV light…), which, in the presence of oxygen, involves an oxidative chain radical process [28,29]. The consequence of (photo)oxidation is a progressive degradation of the properties of PE. Stabilizers are then often used to slow down this process, *e.g.* phenolic antioxidants, Hindered Amine Light Stabilizers (HALS) or UV absorbers [30]. The consequences of the sole morphology modification caused by the MDO drawing on the photodegradation of PE has never been studied so far. However, in a recent work, we reported on the consequences of MDO processing on the solubility of a blooming HALS (Tinuvin® 770) in PE, and the impact on the polymer photostability [27]. It was shown that the solubility of Tinuvin® 770 in PE was increased consecutive to MDO drawing. However, drawn films were more prone to photodegradation in accelerated conditions than undrawn ones. This was attributed to the fact that the total amount of HALS (*i.e.* both soluble and precipitated at the surface) was lower after MDO processing.

While the photodegradation of PE under simultaneous drawing has been extensively reported [31–36], the effect of preliminary orientation on its photostability is more confidential [37–40]. It has been reported that pre-oriented PE samples were less prone to degradation [37,38,40], which has been explained by a decrease in the transport properties of O_2 in the drawn polymer [37]. However, annealing (either with fixed or free ends) led to the same degradability of drawn PE as that of an undrawn film [38].

The work reported here is dedicated to the effect of the MDO drawing on the orientation, crystallinity and permeability of PE films and the consequences of their photoxidation on these features. Orientation caused by the MDO processing was firstly characterized by XRD and polarized FTIR spectroscopy. Crystallinity and oxygen permeability were also assessed prior to photoageing. Photooxidation kinetics of undrawn and drawn films were then compared, and the consequences of photooxidation on crystallinity, orientation and oxygen permeability were studied and correlated to the modification of the polymer structure.

2. Experimental

2.1. Sample composition and preparation

The PE films used hereafter are symmetric three-layer systems (15/70/15 %) that combine one grade of LDPE (density = 0.923 g cm^{-3}, MFI(190 °C, 2.16 kg) = 0.25 g/10 min) and two grades of LLDPE (density = 0.920 g cm^{-3}, MFI(190 °C, 2.16 kg) = 0.50 g/10 min; density = 0.937 g cm^{-3}, MFI(190 °C, 5 kg) = 2.00 g/10 min). They were prepared by Barbier group (Sainte-Sigolène, France) by blown co-extrusion with three extruders A, B and C (screw diameter D = 70, 105 and 70 mm respectively; screw length L = 30 D for all). The films studied here contain no stabilizing agent, except from processing phenolic antioxidants initially present into the raw PE pellets. Reference undrawn films (called "PE-1") were obtained by blown co-extrusion to a final thickness of about 45 μm. MDO-processed films at a draw ratio of 4 ("PE-4") were also manufactured by blown co-extrusion (initial thickness 155 μm) before MDO processing up to a final thickness of about 45 μm. Temperatures of the MDO rolls during drawing are summarized in Table 1.

It should be emphasized that blown extrusion caused some orientation for both PE-1 and PE-4 (*vide infra*) [24], and that undrawn (in the case of PE-1) does not mean non-oriented.

Table 1
Temperature of the rolls used for MDO drawing of the films.

Section of the MDO unit	Roll	Temperature (°C)
Pre-heating (PH)	PH1	75
	PH2	85
Drawing	Slow drive (SD)	88
	Fast drive (FD)	88
Annealing (A)	A1	80
	A2	70
Cooling (C)	C1	60
	C2	30

2.2. Irradiation

Artificial accelerated photoageing of the samples was carried out in a SEPAP MHE device from Atlas. It is composed of a single medium-pressure mercury lamp (1000 W) able to emit light intensities ranging from 90 to 300 W m^{-2} between 290 and 420 nm. Samples are located on a carousel rotating around this central lamp. Two temperature controllers are present within the unit: *i.* a thermocouple located outside the carousel ("Chamber Temperature", CHT), *ii.* a blackbody panel present on the carousel ("Black Standard Temperature", BST). All the experiments were performed at a light intensity of 90 W m^{-2} and a CT/BST couple of 60/70 °C in presence of air.

2.3. Heating

Control experiments were performed in the presence of air within a forced convection oven from Binder regulated at a temperature of 60 °C, comparable to the CHT in the irradiation device.

2.4. Infrared spectroscopy

Fourier-Transform InfraRed (FTIR) spectra (4000-400 cm^{-1}, 32 scans, 2 cm^{-1} resolution) were recorded in transmission mode with a Nicolet 6700 spectrometer from ThermoFisher equipped with a DTGS-KBr detector. Dry air purging is ensured within the analysis chamber in order to remove parasite bands from ambient air (water vapour, carbon dioxide…). Spectra were normalized by the absorbance of the 1378 cm^{-1} band (symmetric bending of end-of-chain $-CH_3$ groups [41]) to compensate for differences in thickness between the samples. Polarized FTIR spectra were obtained by introducing a ZnSe grid polarizer ahead of the samples at two angles (0 and 90°).

2.5. X-ray diffraction

For the preliminary characterization of the structure and the texture of the PE films, a X-Pert Pro diffractometer (Malvern Panalytical) in Bragg Bentano geometry with Cu Kα radiation was used. *FullProf Suite software* [42] was used for the profile refinement of XRD data of samples using the Thompson–Cox–Hastings (TCH) peak profile function. Gaussian contribution was kept constant whatever the direction, while Lorentzian contribution was free to change. NIST SRM LaB_6 standard was used to determine the instrument resolution. The integral breadth method was used to calculate the volume-averaged apparent size of the coherent domains along the [110] and [100] directions considering (110) and (200) reflections respectively [43]. LaB_6 NIST standard was used to correct for instrumental broadening.

The degree of crystallinity χ_c of bulk PE was determined by comparing the area of the amorphous hump to that of the crystalline peaks. The crystallite size was estimated using Scherrer method, which relates the peak broadening of each Bragg peak (βhkl) to a characteristic average volume-weighted domain size D_v in hkl direction. The integral breath β_{hkl} values were obtained from fitting (110) and (200) peaks with a

pseudo-Voigt function using WinPLOTR program and corrected from instrumental broadening using LaB_6 as standard material.

To further probe preferred orientation and crystallization phenomena upon drawing, small and wide-angle X-ray scattering (SAXS/WAXS) measurements were performed on PE films on an Empyrean diffractometer (Malvern Panalytical) with Cu K_α radiation using the line/point collimation setup, an elliptically bent 1D graded focusing mirror, the ScatterX^{78} chamber and the GaliPIX^{3D} detector. Films were clamped on a base holder and the measurements were done in transmission mode perpendicular to the film surface (six scans of 30 min each). Full 2D-WAXS patterns with 360° azimuthal coverage were recorded within a 2θ range from −30.55° to +30.55°. 1D-SAXS patterns were recorded from 0.05° to 8° (q = 0.05–5.68 nm^{-1} where q denotes for the scattering vector $q = 4\pi\sin(\theta)/\lambda$). The 1D-SAXS and 2D-WAXS data were processed using EasySAXS and XRD2Dscan softwares respectively (Malvern Panalytical).

2.6. Thermal analysis

A 3+ Differential Scanning Calorimetry (DSC) apparatus from Mettler Toledo was used for thermal analysis. A heating-cooling-heating cycle (from −20 to 160 °C at 10 °C/min) was applied to samples of 10–15 mg placed into aluminium crucibles and under dry air atmosphere. Melting enthalpy of each sample was compared to that of a 100 % crystalline PE (293 J g^{-1} [44]) to calculate the mass degree of crystallinity χ_c. Thermal history of the polymer was taken into account by using data from the first heating step.

2.7. Oxygen permeability

Oxygen Transmission Rate (OTR) were measured at 23 °C with a 8003 Oxygen Permeation Analyser from Systech Illinois. After complete purge under nitrogen, samples of 5 cm^2 were exposed to pure oxygen (1 atm) in the top part of the analysis chamber, while transmitted oxygen molecules are headed towards a coulometric detector in the bottom part by a flux of oxygen-free nitrogen. OTR (in $cm^3(STP).cm^{-2}.s^{-1}$) were converted into permeability coefficient P (in $cm^{-3}(STP).cm.cm^{-2}.s^{-1}.Pa^{-1}$) to take into account the thickness z of each sample (as well as the difference of oxygen pressure ΔP between the top and bottom parts of the chamber) with:

$$P = \frac{OTR \times z}{\Delta P} \quad \text{Eq. 1}$$

3. Results and discussion

3.1. Effect of the MDO processing

Undrawn PE-1 and MDO-drawn PE-4 were compared prior to photoxidation in terms of orientation (through XRD and polarized FTIR spectroscopy), degree of crystallinity χ_c (determined by XRD and DSC) and oxygen permeability to assess the effect of the MDO drawing process.

3.1.1. Orientation

The XRD patterns in reflection Bragg Brentano geometry of undrawn PE-1 and MDO-drawn PE-4 films prior to photooxidation are shown in Fig. 1. They are typical of semi-crystalline polymers with well-defined high intensity peaks corresponding to the crystalline part, while the amorphous part gives rise to diffuse X-ray scattering and strong halo features at the Bragg peak locations. Peaks that appear at 21.44°, 23.76° and 36.10° correspond, respectively, to the diffraction planes (110), (200) and (020) of the orthorhombic cell of polyethylene in Pnam space group [45]. Orthorhombic and monoclinic are the two main types of unit cells in PE, the former being the most common. In the orthorhombic cell, the macromolecular chains of PE run along the c-axis [5,7] and *hk*0/0*k*0 reflections refer to interchain distances.

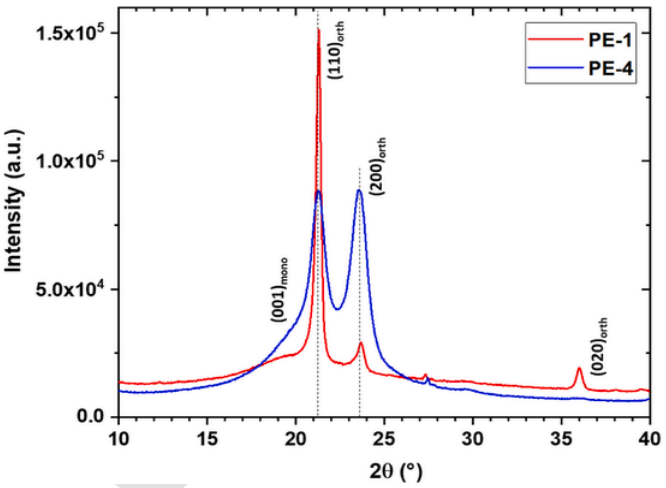

Fig. 1. XRD patterns for undrawn PE-1 (red) and MDO-drawn PE-4 (blue) films prior to photooxidation. $(110)_{orth}$, $(200)_{orth}$, $(020)_{orth}$ represent the (110), (200) and (020) diffraction planes in the orthorhombic PE crystal structure, $(001)_{mono}$ represents the (001) diffraction plane in the monoclinic PE crystal structure. (For interpretation of the references to colour in this figure legend, the reader is referred to the Web version of this article.)

The net increase in FWHM upon drawing clearly shows that the MDO process caused a decrease of the crystallite dimensions, which is confirmed by the calculation of the crystallite size D_v (Table 2). This is consistent with the morphology change reported upon drawing (from spherulitic to fibrillar, *vide supra*) during which lamella are fragmented into smaller crystallites. A reorganization of the in-plane orientation of the chains upon drawing can also be readily seen on the XRD patterns of PE-4 films with the net increase of the intensity of the (200) reflection with respect to the (110) reflection (Table 2). The $I_{(200)}/I_{(110)}$ intensity ratio can be considered as representing a relative orientation, that is often associated to chain drawing, and its increase suggests the formation of an extended chain crystal structure. When the crystallites in a sample are randomly distributed in space, it is known that $I_{(200)}/I_{(110)}$ is in an order of 0.2–0.25 [46]. The value obtained here for the undrawn sample PE-1 around 0.1 indicates a weak (110) orientation, which could be attributed to the blown extrusion process used to prepare the films [24]. On the other hand, the value calculated for the drawn sample PE-4 larger than 1.0 clearly indicates a (200) PE crystal orientation. The increased in PE (200) facet can be usually achieved via high drawing ratio [47]. This is consistent with the fact that drawing of PE often proceeds by alignment of the c-axis of the orthorhombic cell (chain axis) in the drawing direction (here the Machine Direction, MD) [20,22].

Another interesting observation is the presence of a small shoulder at ca. 19.5° in the XRD pattern of the drawn samples, which could be at-

Table 2
Full width at half maximum (FWHM) of (110) and (200) diffraction peaks (Lorentzian L and Gaussian G contributions), average crystallite size D_v in [110] and [200] directions and ratio of integrated intensity $I_{(200)}/I_{(110)}$ of (200) to (110) for undrawn PE-1 and MDO-drawn PE-4 films prior to photooxidation, calculated from XRD Bragg Brentano patterns.

Sample	FWHM (°) L/G		D_v (nm)		$I_{(200)}/I_{(110)}$
	(110)	(200)	[110]	[200]	
PE-1 (undrawn)	0.299/0.047	0.414/0.046	21.5	15.0	0.10
PE-4 (drawn)	1.337/0.047	1.155/0.046	4.3	5.1	1.18

tributed to amorphous scattering in our samples whose degree of crystallinity is lower than 60 %.

2D-WAXS experiments can also be used to qualitatively compare crystal orientation in samples [20–22,24–26,48,49]. The 2D-WAXS patterns of PE films showing diffraction rings of the (110) and (200) lattice planes are displayed in Fig. 2, where the equator and meridian are defined as the horizontal direction (Transverse Direction, TD) and vertical direction (MD), respectively.

Both patterns show two diffusion rings associated to the (110) and (200) planes of the crystallites. The intensity of the rings for PE-1 are homogeneously distributed in space, except for a slight concentration parallel to the MD that can be attributed to the blown extrusion process (*vide supra* [24],). This is consistent with a spherulitic morphology, which was indeed observed by polarized microscopy for PE-1 but not for PE-4 (see Fig. S1 in the ESI). Rings for PE-4, in contrast, are strongly concentrated parallel to the MD. This can be attributed to an orientation of the crystallites with the chain axis oriented preferentially along the MD [20–22,24,26,50]. These results actually reveal the modification of the polymer morphology upon drawing: initial lamellae were broken into smaller crystalline blocks connected by amorphous chains oriented along the MD in the fibrillar structure.

For a quantitative examination of crystal orientation, the corresponding azimuthal intensity curves of the (110) and (200) lattice planes are also shown in Fig. 3 where the azimuthal angles of 0° (180°) and 90° (270°) are defined as the equator and meridian directions, respectively.

Although of low intensity, the observation of distinct peaks on the azimuthal scans for undrawn samples confirms the weak orientation of PE in them (Fig. 3a). The maximum intensity of (110) was found to locate at about 30° relative to the equator, and the maximum intensity of (200) was found in the meridian region with zero scattering on the equator. A change in crystal orientation is observed upon drawing, with crystals oriented along the equator as evidenced by the observation of two sharp and intense peaks at 0° and 180° in the (110) azimuthal distribution (Fig. 3b). The maximum intensity of (200) was also found in

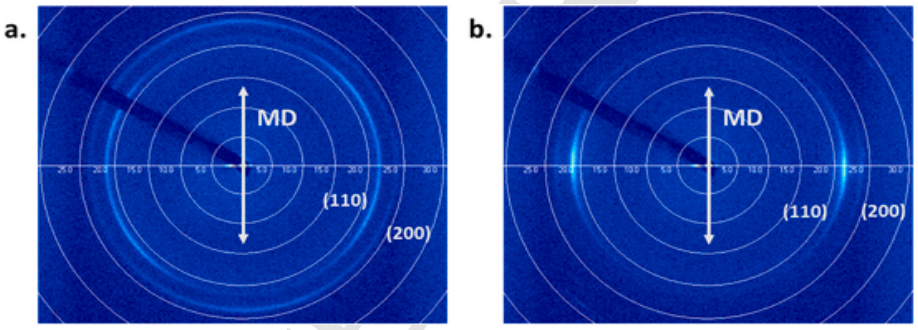

Fig. 2. 2D-WAXS patterns of a. undrawn PE-1, b. MDO-drawn PE-4 prior to photooxidation. Direction of drawing (Machine Direction, MD) is represented by a white arrow.

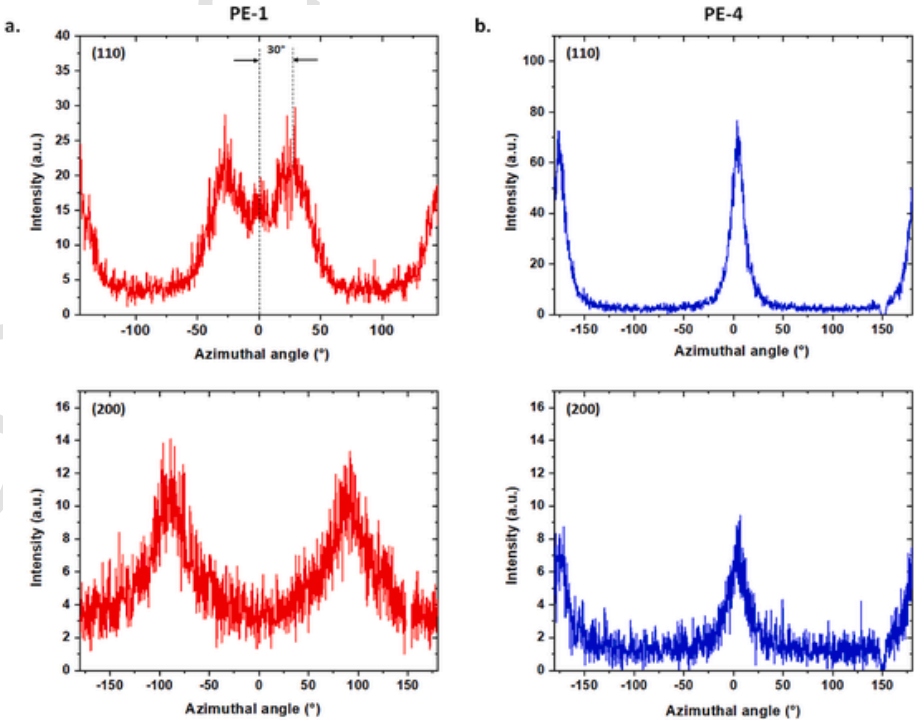

Fig. 3. Intensity profiles along the azimuthal angle of (110) and (200) diffraction planes extracted from the 2D-WAXS patterns of a. undrawn PE-1, b. MDO-drawn PE-4 films prior to photooxidation.

the equator region with no more visible scattering intensity at the meridian.

The arrangement of both (110) and (200) diffractions in the direction vertical to the drawing direction MD demonstrates a c-axis orientation of the PE crystals along the drawing direction, that is consistent with the reported morphological change from spherulitic to fibrillar. It was not possible to determine the crystalline axis orientation factors from 2D-WAXS patterns because of the low signal to noise ratio measured.

In addition to XRD, it is also possible to quantify the orientation of chains with respect to the MD by calculating the orientation function $f_{c,MD}$ (Eq. (2)) using polarized FTIR spectroscopy [20,26,48,49,50]:

$$f_{c,MD} = \frac{3\cos^2(\phi_{c,MD}) - 1}{2} \quad \text{Eq. 2}$$

$\phi_{c,MD}$ represents the angle between the c-axis of the unit cell (hence the polymer chains) and the MD. $f_{c,MD}$ values range between −0.5 ($\phi_{c,MD} = 90°$) and 1 ($\phi_{c,MD} = 0°$).

Calculation of $f_{c,MD}$ can be carried out using the dichroic ratio D determined from polarized FTIR experiments with Eqs. (3) and (4).

$$D = \frac{A_{\parallel}}{A_{\perp}} \quad \text{Eq. 3}$$

$A_{\parallel}$ and $A_{\perp}$ represent the absorbances taken from a spectrum recorded with IR light polarized parallel and perpendicular, respectively, to the MD.

$$f_{i,MD} = \frac{2}{3\cos^2(\alpha) - 1}\frac{(D-1)}{(D+2)} \quad \text{Eq. 4}$$

with α the angle between the transient dipole moment of the vibration and the i-axis [48,49].

For PE, the intense 720/730 cm^{-1} bands (Fig. 4) can be used for this purpose, as their transition dipole moments are oriented along the b- and a-axis respectively (*i.e.* α = 0° in Eq. (4)) [51–54]. It enables the calculation of $f_{b,MD}$ and $f_{a,MD}$ respectively, from which $f_{c,MD}$ can be deduced with the orthogonality relation [49]:

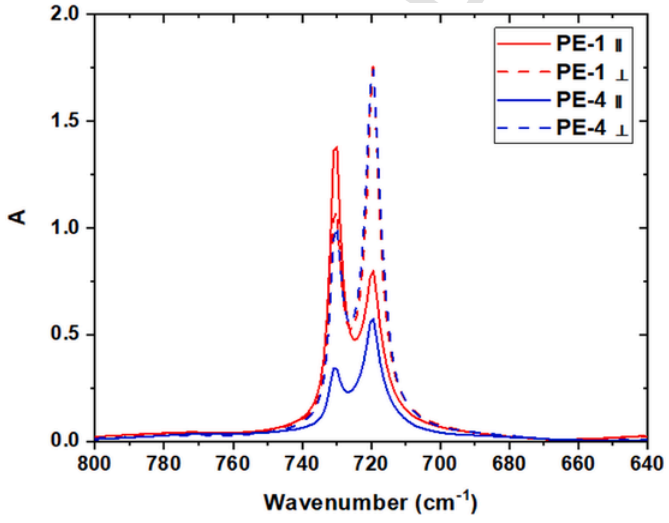

Fig. 4. Polarized FTIR spectra in the 800-640 cm^{-1} region prior to photooxidation for undrawn PE-1 (red) and MDO-drawn PE-4 (blue) films with IR polarization parallel (solid) or perpendicular (dashed) with respect to the MD. (For interpretation of the references to colour in this figure legend, the reader is referred to the Web version of this article.)

$$f_{a,MD} + f_{b,MD} + f_{c,MD} = 0 \quad \text{Eq. 5}$$

It can be observed in Fig. 4 that the ratio between $A_{\parallel}$ and $A_{\perp}$ for the 720/730 cm^{-1} bands measured for PE-1 and PE-4 are different. This evidences a different orientation of the chains into the two samples. As this complex broad band is actually a convolution of two crystalline bands located at around 720 and 730 cm^{-1} and an amorphous one at 723 cm^{-1} [55], the calculation of the dichroic ratio required at first a mathematical curve-fitting (see details in the ESI). Results of $f_{a,MD}$, $f_{b,MD}$ and $f_{c,MD}$ are reported in Table 3. Values of $f_{c,MD}$ thus obtained are similar to those calculated from the crystalline bands at 1051 (–CH_2– twisting, α = 0°) and 1896 cm^{-1} (combination of –CH_2- rocking modes at 1168 cm^{-1} and 720/730 cm^{-1}, α = 90°) [56,57], which can be used without any mathematical treatment of the spectra but suffer from low absorbance values (Table S1). Orientation factors $f_{i,MD}$ calculated here are consistent with those reported in [24] for a blown-extruded film prior and after MDO processing at a draw ratio of 4.

It can be observed that $f_{b,MD}$ remained constant from PE-1 to PE-4, while $f_{a,MD}$ decreased and $f_{c,MD}$ increased. Similar changes have been reported for MDO-drawn films in [20,24], with a- and b-axis preferentially oriented along Normal Direction (ND) and Transverse Direction (TD), respectively, upon drawing [25]. Upon MDO processing, a- and c-axis then rotated around b-axis in opposite directions with respect to the MD (respectively opposite to and toward the MD). Decrease of $f_{a,MD}$ upon MDO drawing is one of the characteristics of roll-to-roll drawn films, while increase of $f_{c,MD}$ confirms that MDO processing leads to an orientation of the c-axis of the orthorhombic unit cell (*i.e.* the polymer chains) along the drawing direction.

3.1.2. Degree of crystallinity

MDO processing of PE films has often been associated with a moderate increase of their degree of crystallinity caused by stress-induced crystallization [20–22], seldom the absence of any change [25]. The degree of crystallinity χ_c (Table 4) was calculated in the present case from DSC (ratio of the melting enthalpy to that of a 100 % crystalline PE [44]) and XRD experiments (calculated by considering the integrated intensity of the features related to the amorphous and crystalline components). Within the experimental error, results from DSC and XRD are consistent with each other and show that the degree of crystallinity of our samples was not affected by the MDO processing.

3.1.3. Oxygen permeation

The mechanism of permeation can be decomposed into three consecutive steps: *i.* solubilization of the penetrant at the polymer surface, *ii.* diffusion from the entrance to the exit surface, *iii.* desorption at the latter. The first and third steps are associated with the thermodynamic solubility coefficient S, while the second one is related to the kinetic dif-

Table 3
Orientation factors *f* with respect to the MD from polarized FTIR spectroscopy for undrawn PE-1 and MDO-drawn PE-4 films prior to photooxidation.

Sample	Orientation factors $f_{i,MD}$		
	$f_{a,MD}$	$f_{b,MD}$	$f_{c,MD}$
PE-1 (undrawn)	0.10	−0.27	0.17
PE-4 (drawn)	−0.32	−0.32	0.64

Table 4
Degree of crystallinity χ_c calculated from DSC and XRD experiments for undrawn PE-1 and MDO-drawn PE-4 films prior to photooxidation.

	Degree of crystallinity χ_c (wt%)	
	DSC	XRD
PE-1 (undrawn)	51	47
PE-4 (drawn)	51	42

fusion coefficient D [58–61]. The ability of a penetrant to cross a polymer film is ultimately represented by its permeability coefficient P defined as:

$$P = D \times S \quad \text{Eq. 6}$$

It has been demonstrated that crystalline regions are so densely packed that they are impermeable, which restricts both the sorption and the diffusion to the amorphous regions of semi-crystalline polymers such as PE [62]. As a consequence, S can be expressed as a function of the volume degree of crystallinity χ_c by:

$$S = S_a (1 - \chi_c) \quad \text{Eq. 7}$$

with S_a the solubility coefficient of the amorphous phase. From the fractional free volume (FFV) theory [63], S_a can be defined as:

$$S_a = \frac{f_a}{f_1 \, p_T \, \exp\,(1 + \chi_1)} \quad \text{Eq. 8}$$

f_a stands for the fractional free volume of the amorphous part, f_1 for the fractional free volume of the penetrant, p_T for the liquid-vapour equilibrium pressure of the gas and χ_1 for the Flory-Huggins parameter of the (penetrant-polymer) system.

In addition, the presence of crystallites restricts the diffusion of the penetrant molecules as a consequence of the tortuosity and the limitation in mobility of the amorphous chains close to the crystalline regions [62]. These two effects are considered in the FFV theory through the tortuosity factor τ and the immobilization factor β respectively [63].

$$D = \frac{D_a}{\tau\beta} = \frac{A}{\tau\beta} \exp\left(\frac{-b\nu^*}{f_a}\right) \quad \text{Eq. 9}$$

with D_a the diffusion coefficient of the amorphous phase, A and b parameters specific to a penetrant-polymer couple and ν^* the critical hole size for diffusion.

The oxygen permeability coefficient P was determined for PE-1 (1.18×10^{-13} $cm^3(STP).cm.cm^{-2}.s^{-1}.Pa^{-1}$) and PE-4 ($0.82 \times 10^{-13}$ $cm^3(STP).cm.cm^{-2}.s^{-1}.Pa^{-1}$) prior to photooxidation. The MDO-processed film is then 30 % less permeable than its undrawn equivalent. Such an effect has been often reported for PE upon uniaxial drawing [64,65], more scarcely upon specific MDO processing [22,66]. It has been explained by several phenomena caused by drawing: *i.* increase of the degree of crystallinity, *ii.* increase of tortuosity through the fragmentation of lamellae into smaller crystalline blocks, *iii.* increase of density of the amorphous phase (hence decrease of f_a). In the present case, no change of the degree of crystallinity was observed between PE-1 and PE-4, so the decrease of permeability upon drawing would rather be owing to an enhancement of the tortuosity consecutive to the MDO drawing and/or a decrease in the amorphous phase density.

3.2. Effect of photooxidation on undrawn and MDO-drawn PE films

3.2.1. Kinetics of photooxidation

To assess the effect of MDO on the photooxidation of polyethylene, PE-1 and PE-4 films were exposed to light irradiation in the SEPAP MHE device at 90 W m^{-2} up to 200 h and FTIR spectra were regularly recorded. The formation of several oxygen-containing functions resulting from the photooxidation of PE can be observed in the 1900-1500 cm^{-1} region (Fig. 5): carboxylic acids (1713 cm^{-1}), esters (1735 cm^{-1}) and lactones (1780 cm^{-1}), as well as alcohols and hydroperoxides (broad band with a maximum at 3420 cm^{-1}) [28]. The shape of the carbonyl envelop was identical for PE-1 and PE-4, which indicates that the stoichiometry of the oxidation products was not altered by the modification of the morphology and that the modifications induced by the MDO processing (especially the chain orientation, *vide supra*) did not modify the photooxidation mechanism.

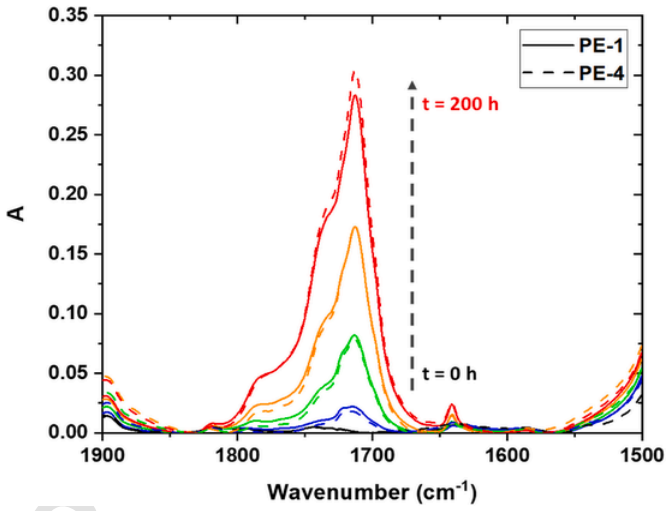

Fig. 5. FTIR spectra in the 1900-1500 cm^{-1} region upon photooxidation for undrawn PE-1 (solid) and MDO-drawn PE-4 (dashed) films – I = 90 W m^{-2}, CHT/BST = 60/70 °C.

The difference of absorbance ΔA at 1713 cm^{-1} (C═O symmetric stretching in carboxylic acids [41]) with respect to the unexposed film is plotted as a function of photooxidation time in Fig. 6 for both PE-1 and PE-4. Thermal ageing experiments at 60 °C without light (dark control) for the same time (200 h) did not show any change in the FTIR spectra, which evidenced the photochemical origin of the oxidation mechanism at this time scale.

Despite the change in morphology and the orientation of the polymer chains along the MD caused by the MDO drawing, no difference in the photooxidation kinetics was observed between PE-1 and PE-4. This can be explained by the occurrence of an annealing step during the MDO process. Indeed, it was reported that annealing partly cancels the beneficial effect of orientation on the photostability of PE [38]. MDO

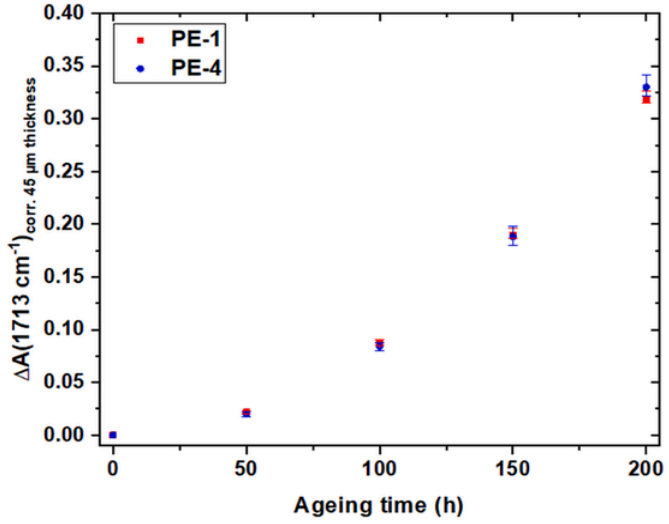

Fig. 6. Difference of absorbance at 1713 cm^{-1} with respect to unexposed film for undrawn PE-1 (red square) and MDO-drawn PE-4 (blue circle) films as a function of photooxidation time – I = 90 W m^{-2}, CHT/BST = 60/70 °C. Results are an average from 3 samples, error bars correspond to minimum and maximum values. ΔA values are corrected for having 45 µm thickness for all samples. (For interpretation of the references to colour in this figure legend, the reader is referred to the Web version of this article.)

drawing thus enhances several properties of PE, including its capacity to act as a barrier to oxygen, without degrading its durability.

3.2.2. Change in crystallinity upon photooxidation

As can be seen in Table 5, a small variation of FWHM of the (110) and (200) Bragg peaks as a function of the photooxidation time was observed within each series. It reveals an increase in the size of the crystallites upon photooxidation, which is confirmed by the D_v values calculated from the (110) and (200) peaks after 200 h of ageing.

The degree of crystallinity χ_c from DSC and XRD in the course of photooxidation is represented in Fig. 7. As can be observed, it remains constant up to 100 h before a slight increase for both PE-1 and PE-4 samples. This increase may be explained by the chemicrystallization process [29,67]: shorter and more mobile chains are produced by chain scissions upon (photo)ageing in the amorphous regions and can then crystallize. The increase of the crystallite size observed (Table 5) is then in favor of a chemicrystallization process that would rather involve the thickening of existing crystallites rather than the formation of new ones. The similar increase of χ_c for both PE-1 and PE-4 is consistent with the alike kinetics of photooxidation shown above.

Finally, 1D-SAXS profiles were recorded on undrawn PE-1 and MDO-drawn PE-4 prior and after 200 h of photoageing (Fig. 8). A broad peak is only observed for PE-1 after 200 h of photooxidation. It indicates a stacked lamellar structure for this sample, with a q_{max} value of about 0.257 nm^{-1} leading to a long period $L_p = 2\pi/qmax = 24.5$ nm. Given the small changes previously observed in crystallite sizes and degree of crystallinity, this peak would be better attributed to a reorganization of the amorphous part of the polymer upon photoageing.

In addition, a small shoulder can be observed for PE-1 at 0 h. This might correspond to the long period and Lorentz correction was then applied in order to reveal it (insert of Fig. 8). However, even with this correction, it was not possible to confirm the presence of a peak for PE-1 at 0 h because of the noise on the data points.

Table 5
Full width at half maximum (FWHM) of (110) and (200) diffraction peaks (Lorentzian L and Gaussian G contributions) and average crystallite size D_v in [110] and [200] directions for undrawn PE-1 and MDO-drawn PE-4 films after different photooxidation times, calculated from XRD Bragg Brentano patterns.

Sample	Photooxidation time (h)	FWHM (°) L/G		D_v (nm)	
		(110)	(200)	[110]	[100]
PE-1 (undrawn)	0	0.299/0.047	0.414/0.046	21.5	15.0
	100	0.280/0.047	0.365/0.046	23.2	17.3
	200	0.274/0.047	0.382/0.046	23.8	16.5
PE-4 (drawn)	0	1.337/0.047	1.155/0.046	4.3	5.1
	100	0.842/0.047	0.870/0.046	7.1	6.8
	200	0.851/0.047	0.794/0.046	7.0	7.5

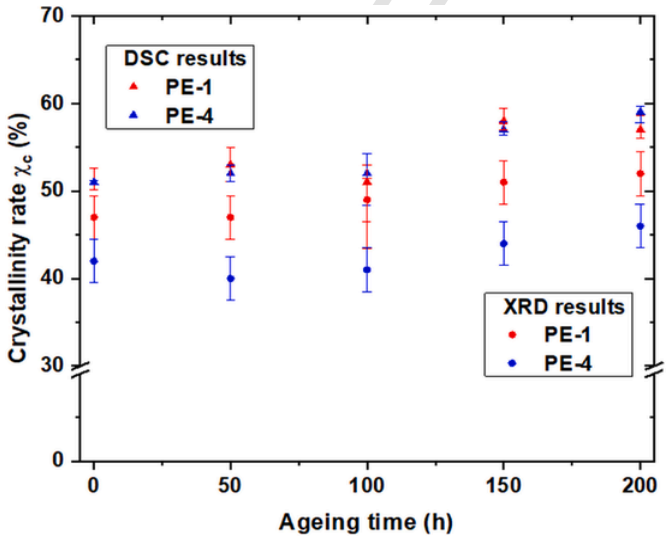

Fig. 7. Degree of crystallinity χ_c for undrawn PE-1 (red) and MDO-drawn PE-4 (blue) films determined from DSC (triangle) and XRD (bullet) as a function of photooxidation time – I = 90 W m^{-2}, CHT/BST = 60/70 °C. Results are an average from 3 samples, error bars correspond to minimum and maximum values. (For interpretation of the references to colour in this figure legend, the reader is referred to the Web version of this article.)

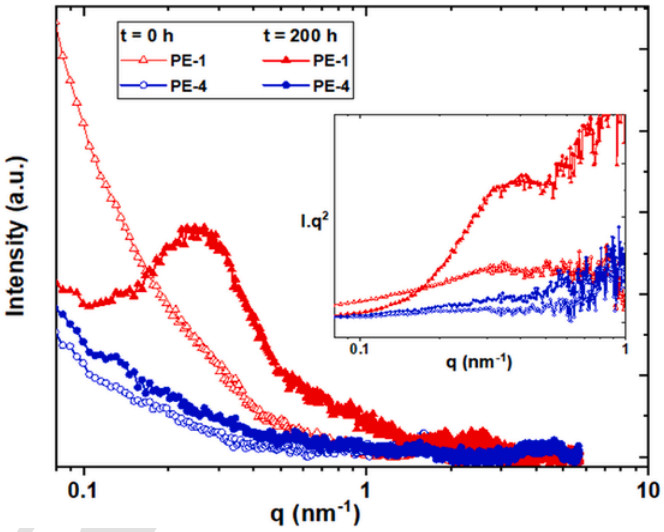

Fig. 8. 1D-SAXS profiles for undrawn PE-1 (red triangles) and MDO-drawn PE-4 (blue circles) at 0 h (open) and 200 h (plain) of photooxidation – I = 90 W m^{-2}, CHT/BST = 60/70 °C. Insert: Lorentz corrected SAXS data $I.q^2$ *vs.* q. (For interpretation of the references to colour in this figure legend, the reader is referred to the Web version of this article.)

3.2.3. Modification of orientation upon photooxidation

No significant shift in the XRD peak position of the crystalline part was observed for PE-1 and PE-4 upon photooxidation (see results in the ESI). The $I_{(200)}/I_{(110)}$ ratio slightly decreased within the first 50 h of ageing (*e.g.* from 1.18 to 1.07 for PE-4), but was then constant (Table S2).

Changes of the orientation function $f_{c,MD}$ (as well as $f_{a,MD}$ and $f_{b,MD}$) were also evaluated during the photooxidation using the absorbance of the IR bands at 720 and 730 cm^{-1}. Orientation functions with respect to the MD are plotted for a- and c-axis in Fig. 9 ($f_{b,MD}$ being constant all along the photooxidation). The absence of any change in $f_{b,MD}$ reveals that the orientation of this axis with respect to the MD was not modified by photooxidation.

It can be observed that $f_{a,MD}$ and $f_{c,MD}$ were slightly modified in opposite directions after 50 h of light exposure for both samples, before reaching a constant value up to the final photooxidation time.

The only changes in orientation ($I_{(200)}/I_{(110)}$ ratio, $f_{a,MD}$ and $f_{c,MD}$) occurred within the first 50 h of photooxidation, which corresponds to ΔA (1713 cm^{-1}) < 0.025. They cannot thus be explained by the photoageing process but rather by some physical ageing (*i.e.* reorganization of the amorphous part of the polymer which also affect the orientation of the neighboring crystalline part). This could occur upon exposure to temperature (60 °C) into the accelerated photoageing device prior to the onset of the photochemical ageing mechanism. The absence of any change after 50 h reveals that the photooxidation process does not have any effect on the orientation of the crystallites.

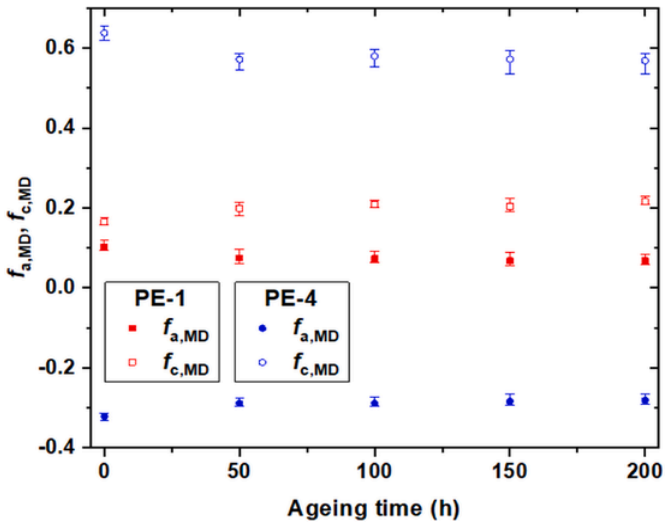

Fig. 9. Orientation functions $f_{a,MD}$ and $f_{c,MD}$ as a function of photooxidation time for undrawn PE-1 and MDO-drawn PE-4 films – I = 90 W m^{-2}, CHT/BST = 60/70 °C. Results are an average from 3 samples, error bars correspond to minimum and maximum values.

In addition, orientation of amorphous chains was studied upon photooxidation by calculating $f_{c,MD}$ at 1368 and 1352 cm^{-1}. Except for a small decrease at 50 h, no change was observed (Fig. S5 in the ESI).

3.2.4. Modification of permeability upon photooxidation

Despite the crucial role of this parameter in numerous applications, the change of permeability upon photoageing has only received little attention up to now [68–76]. Fig. 10a shows the changes of the permeability coefficient P along photooxidation for both PE-1 and PE-4 (results for the dark control experiment are plotted in Fig. 10b).

As can be seen in Fig. 10, the permeability coefficient P slightly increased during the first 50 h for both photochemical and thermal ageing conditions. P remained then constant up to 200 h for thermal experiments (Fig. 10b), whereas it linearly decreased under light exposure (Fig. 10a). In the latter case, the decrease rate appears to be higher for PE-1 (−35 % from initial value after 200 h) than PE-4 (−25 %), to such an extent that P is close for both samples after 200 h. From the point of view of barrier properties, these results suggest that photooxidation has a beneficial role on PE barrier properties, as it progressively reduces the permeability to oxygen. By comparing the change of P upon photooxidation to that during thermal ageing, it appears that the initial increase of the oxygen permeability (first 50 h) is rather a thermal effect than a photochemical one as it occurs in both cases. It may be associated to a slight reorganization induced by physical ageing, which was previously evidenced in the orientation experiments (*vide infra*). However, it is obvious that the decrease of P observed in a second time is of photochemical origin, as it only appeared in presence of light, and is then a consequence of the photooxidation process. Decrease in oxygen permeability could cause the photooxidation to slow down or even stop because of oxygen starvation. Nevertheless, these conditions are not reached here, as can be seen in the photooxidation kinetics of Fig. 6.

Crystallites are so densely packed that they are impermeable to oxygen. As a consequence, permeation and then photooxidation are both restricted to the amorphous part of a polymer [29,62]. From a general point of view, and as reported above in the manuscript, photooxidation may affect the polymer structure in several ways: *i.* crystallinity could be modified through chemicrystallization [29,67], *ii.* polar functions such as hydroxyls, carboxylic acids, esters, etc. are formed [28–30], *iii.* chain scissions can occur, which increase the macromolecular mobility, *iv.* crosslinks could appear [29]. All these effects would affect the permeability of a polymer. Indeed, chemicrystallization would cause a decrease of both S (Eq. (7)) [62] and D (increased tortuosity and chain immobilization, Eq. (9)) [62,63]. The formation of polar groups may modify the interactions between the polymer and the permeant (change in χ_1 causing a modification of S_a, see Eq. (8)) and the cohesion energy density of the polymer (change in D). Chain scissions could ease the diffusion process, while crosslinking would have the opposite effect [60].

As presented above, the degree of crystallinity increases upon photoageing (Fig. 7), while polar groups appeared within the polymer structure (Fig. 5). Steric Exclusion Chromatography (SEC) analyses were performed on PE-1 and PE-4 at different stages of photooxidation (0, 50 and 200 h, see results in the ESI). Mass average molar masses $\overline{M}_w$ are initially similar for PE-1 and PE-4 (about 450 000 g mol^{-1}) and a high polydispersity was observed for both samples prior to ageing (I_p = 27). High initial polydispersity was not surprising as the samples are composed of different grades of LDPE and LLDPE. Upon photoageing, the same behavior is observed for PE-1 and PE-4: chromatograms reveal a decrease of $\overline{M}_w$ up to 62 000 g mol^{-1} after 200 h of photoageing, with a huge decrease of polydispersity (up to I_p = 7 at 200 h). This decrease of $\overline{M}_w$ clearly shows the occurrence of chain scissions, what is confirmed by the decrease of I_p. In addition, there is no evidence of any crosslinking upon photoageing as no signal of higher molar mass was observed in the chromatograms and no insoluble fraction was detected in gel fraction experiments.

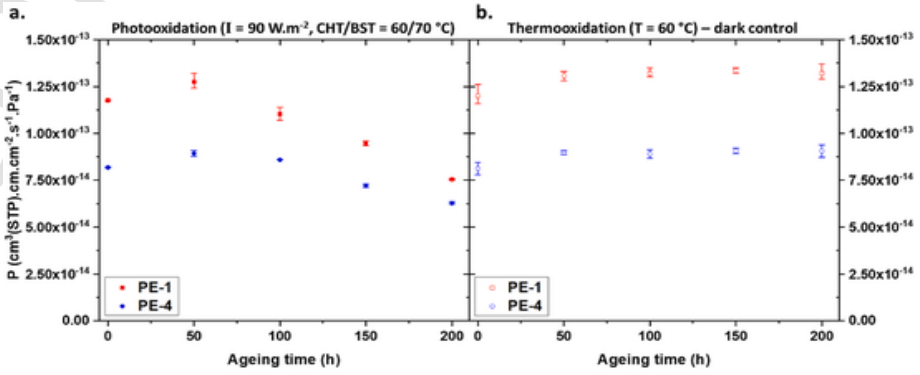

Fig. 10. Permeability coefficient P for undrawn PE-1 (red square) and MDO-drawn PE-4 (blue circle) films as a function of ageing time upon a. photooxidation, b. thermooxidation. Results are an average from 3 samples, error bars correspond to minimum and maximum values. (For interpretation of the references to colour in this figure legend, the reader is referred to the Web version of this article.)

The marginal increase of the degree of crystallinity observed for both samples upon photooxidation would not be able to explain, on its own, the extent of the decrease of P with Eq. (7), so other factors might have an effect. The increase of tortuosity brought by the chemicrystallization process would be involved. Indeed, this phenomenon involves, in the present case, the addition of short macromolecules resulting from chain scissions to existing crystallites, which could further hinder the diffusion of oxygen (Eq. (9)). This effect may be more important for PE-1 whose morphology is of spherulitic nature than for PE-4 composed of fibrils constituted by small crystalline blocks connected by amorphous chains and whose tortuosity is initially higher. This would explain the higher decrease of P for PE-1 than PE-4. The formation of polar groups in apolar PE upon photooxidation would also participate to the reduction of P. Indeed, this would hinder the interactions between PE and apolar oxygen (increased χ_1 causing a decrease of S_a, see Eq. (8)), and increase the cohesion energy density of the polymer (reduced D). The contribution of chain scissions to the change in oxygen permeability seems minor as P decreased. However, it is difficult to discriminate these effects as they occur simultaneously during the photooxidation of PE and would not have the same relative impact on the change in permeability.

4. Conclusion

XRD and polarized FTIR spectroscopy showed that Machine Direction Orientation (MDO) drawing resulted in the transformation of the initial spherulitic structure of PE into an oriented fibrillar morphology composed of fragmented crystalline blocks linked by amorphous chains oriented along the drawing direction. No modification of the degree of crystallinity was caused by the MDO process, but a 30 % reduction of the oxygen permeability was observed. This can be explained by an increase of the amorphous phase density and of the tortuosity (caused by the smaller crystalline blocks resulting from the fragmentation of the initial lamellae) in the fibrillar morphology.

Undrawn (PE-1) and MDO-drawn (PE-4) films presented identical photooxidation kinetics. This could be attributed to the annealing step of the MDO process which cancels the reported beneficial effect of orientation on the photostability of PE. The stoichiometry of the oxidation products was not affected by the change in morphology between PE-1 and PE-4. The degree of crystallinity of both samples increased upon photooxidation owing to the chemicrystallization mechanism, and, as the crystallite size increased during the photooxidation process, it can be concluded that it occurred through the growth of existing crystallites. The polymer orientation slightly changed during the first 50 h of photoageing, which could be due to physical ageing, but then stayed constant up to complete photooxidation. Oxygen permeability of both undrawn and MDO-drawn films showed a slight initial increase (which could be also explained by physical ageing) followed by a continuous decrease due to the photooxidation process. Indeed, photooxidation has consequences on the chemical structure and morphology of PE that could modify its permeability. The formation of polar functions, evidenced by FTIR spectroscopy, would on one hand increase the polymer cohesion energy density and on the other hand reduce its affinity with apolar molecular oxygen, resulting in a decrease of the oxygen permeability. Moreover, the observed change in crystallinity caused by chemicrystallization would reduce the amount of permeable material (as crystalline regions are considered impermeable) and increase the tortuosity, also reducing the oxygen permeability. As for chain scissions, which were evidenced upon photooxidation by SEC experiments, they would increase the permeability. However, they did not prevail over the increase in polarity and the chemicrystallization process because the oxygen permeability is, on the whole, decreasing upon photooxidation. It would be of great interest to distinguish between these effects on the permeability by considering polar permeants (such as water vapour) instead of apolar oxygen, as well as determine values of the solubility and diffusion coefficients upon photooxidation to assess if these steps are affected in the same manner upon photoageing.

CRediT authorship contribution statement

Julien Christmann: Writing – original draft, Supervision, Investigation, Conceptualization. **Christine Taviot-Guého:** Writing – review & editing, Investigation. **Emma Mazeau:** Investigation. **Jean-Luc Gardette:** Writing – review & editing, Supervision, Funding acquisition, Conceptualization. **Gérard Pichon:** Resources. **Bruno Bouchut:** Writing – review & editing, Resources. **Sandrine Therias:** Writing – review & editing, Supervision, Funding acquisition, Conceptualization.

Declaration of competing interest

The authors declare that they have no known competing financial interests or personal relationships that could have appeared to influence the work reported in this paper.

Acknowledgements

The authors wish to thank ANR for financial support within the framework of the ANR-Labcom POPBA project. F. Schiavi and N. Bolfan (LMV, Université Clermont Auvergne) are fully acknowledged for the loan of their IR grid polarizer.

Data availability

Data will be made available on request.

Appendix A. Supplementary data

Supplementary data to this article can be found online at https://doi.org/10.1016/j.polymer.2024.127692.

References

[1] Plastics – the Facts 2022, Plastics Europe, 2022.
[2] D.R. Breese, E. Hatfield, in: K.L. Yam (Ed.), The Wiley Encyclopedia of Packaging Technology, third ed., Wiley, Hoboken NJ, 2009, p. 685.
[3] D.R. Breese, Benefits of machine direction-oriented films in flexible-packaging applications, Convert Q (Quarter 2) (2011) 32–36.
[4] E. Hatfield, in: J.R. Wagner (Ed.), Multilayer Flexible Packaging, second ed., Elsevier, Oxford, 2016, p. 147.
[5] A.J. Peacock, Handbook of Polyethylene – Structures, Properties, and Applications, Marcel Dekker, Inc., New York, 2000, p. 415.
[6] Z. Bartczak, A. Galeski, Plasticity of semicrystalline polymers, Macromol. Symp. 294–1 (2010) 67–90.
[7] L. Lin, A.S. Argon, Structure and plastic deformation of polyethylene, J. Mater. Sci. 29 (1994) 294–323.
[8] P.B. Bowden, R.J. Young, Deformation mechanisms in crystalline polymers, J. Mater. Sci. 9 (1974) 2034–2051.
[9] R. Séguéla, Plasticity of semi-crystalline polymers: crystal slip versus melting-recrystallization, E-Polymers 7 (2007) 1–17.
[10] W.W. Adams, D. Yang, E.L. Thomas, Direct visualization of microstructural deformation processes in polyethylene, J. Mater. Sci. 21 (1986) 2239–2253.
[11] A. Peterlin, Crystalline character in polymers, J. Polym. Sci. C 9 (1965) 61–89.
[12] A. Peterlin, Molecular model of drawing polyethylene and polypropylene, J. Mater. Sci. 6 (1971) 490–508.
[13] A. Peterlin, The composite structure of fibrous material, Adv Chem Ser 142 (1975) 1–13.
[14] A. Peterlin, Drawing and extrusion of semi-crystalline polymers, Colloid Polym. Sci. 265 (1987) 357–382.
[15] K. Sakaoku, A. Peterlin, Surface replicas of drawn polyethylene. II. Annealing of cold-drawn samples with different draw ratio, J Macromol Sci B1 1 (1967) 103–118.
[16] G. Capaccio, I.M. Ward, Fibrillar structure of ultra-oriented polyethylene, Polymer 18 (1977) 967–968.
[17] A.J. Owen, Scanning electron microscopy of oriented high density polyethylene, Colloid Polym. Sci. 259 (1981) 252–259.
[18] M. Furuta, S. Hosoda, K. Kojima, Study of deformation mechanism for linear low-density polyethylene, J. Appl. Polym. Sci. 33 (1987) 401–410.
[19] E. Hatfield, R. Tate, K. Williams, W. Todd, New MDO medium molecular weight

high density polyethylene films, J. Plast. Film Sheeting 18 (2002) 117–127.
[20] S.H. Tabatabaei, L. Parent, P. Cigana, A. Ajji, P.J. Carreau, Effect of machine direction orientation conditions on properties of HDPE films, J. Plastic Film Sheeting 25 (2009) 235–249.
[21] T. Chatterjee, R. Patel, I.V.J. Garnett, R. Paradkar, S. Ge, L. Liu, Jr.KT. Forziai, N. Shah, Machine Direction Orientation of high density polyethylene (HDPE): barrier and optical properties, Polymer 55 (2014) 4102–4115.
[22] S. Srinivas, P. Brant, Y. Huang, D.R. Paul, Structure and properties of oriented polyethylene films, Polym. Eng. Sci. 43 (2003) 831–849.
[23] Schut JH. MDO films: Lots of promise, big challenges. Plastics Technology, available online at https://www.ptonline.com/articles/mdo-films-lots-of-promise-big-challenges (consulted on the 21/07/2023)..
[24] A. Bafna, D. McFaddin, G. Beaucage, J. Merrick-Mack, F.M. Mirabella, Integrated mechanism for the morphological structure development in HDPE melt-blown and Machine-Direction-Oriented films, J. Polym. Sci. B 45 (2007) 1834–1844.
[25] V. Ratta, G.L. Wilkes, T.K. Su, Structure-property-processing investigations of the tenter-frame process for making biaxially oriented HDPE film. I. Base sheet and draw along the MD, Polymer 42 (2001) 9059–9071.
[26] D.R. Breese, G. Beaucage, Modelling the mechanical properties of highly oriented polymer films: a fibre/gel composite theory approach, J. Polym. Sci. B 46 (2008) 607–618.
[27] J. Christmann, J.-L. Gardette, G. Pichon, B. Bouchut, S. Therias, Photostabilization of polyethylene by a hindered amine light stabilizer in blooming conditions and impact of MDO processing, Polym Degrad Stab 191 (2021) 109683.
[28] M. Gardette, A. Perthué, J.-L. Gardette, T. Janescka, E. Földes, B. Pukánszky, S. Therias, Photo- and thermal-oxidation of polyethylene: comparison of mechanisms and influence of unsaturation content, Polym Degrad Stab 98 (2013) 2383–2390.
[29] J.F. Rabek, Photodegradation of Polymers, Springer-Verlag, Berlin Heidelberg, 1996.
[30] F. Gugumus, in: G. Scott (Ed.), Mechanism of Polymer Degradation and Stabilisation, Elsevier Applied Science, Barking, 1990, p. 169.
[31] F.S. Kaufman Jr, A new technique for evaluating outdoor weathering properties of high density polyethylene, Appl. Polym. Symp. 4 (1967) 131–139.
[32] D. Benachour, C.E. Rogers, in: S.P. Pappas, F.H. Winslow (Eds.), Photodegradation and Photostabilization of Coatings, American Chemical Society, Washington DC, 1981, p. 263.
[33] D. Benachour, C.E. Rogers, in: C.G. Gebelein, D.J. Williams, R.D. Deanin (Eds.), Polymers in Solar Energy Utilization, American Chemical Society, Washington DC, 1983, p. 307.
[34] L. Peeva, S. Evtimova, Effect of mechanical stress on oxidation of polymers, Eur. Polym. J. 20 (1984) 1049–1051.
[35] W.K. Busfield, P. Taba, Photo-oxidative degradation of mechanically stressed polyolefins, Polym Degrad Stab 51 (1996) 185–196.
[36] D.R. Tyler, Mechanistic aspects of the effect of stress on the rates of photochemical degradation reactions in polymers, J Macromol Sci C 44 (2004) 351–388.
[37] G. Akay, T. Tinçer, E. Aydin, The effect of orientation on the radiation induced degradation of polymers, Eur. Polym. J. 16 (1980) 597–600.
[38] G. Akay, T. Tinçer, The effect of orientation on radiation-induced degradation in high-density polyethylene, Polym. Eng. Sci. 21 (1981) 8–17.
[39] S.S. Stivala, L. Reich, Structure vs stability in polymer degradation, Polym. Eng. Sci. 20 (1980) 654–661.
[40] A. Tanaka, E. Miyagawa, H. Uno, M. Kitamura, K.-H. Nitta, Influence of morphology on photo-degradation of low-density polyethylene films, Polym. Eng. Sci. 40 (2000) 2007–2013.
[41] G. Socrates, Infrared and Raman characteristic group frequencies. Tables and Charts, third ed., Wiley, Chichester, 2001.
[42] J. Rodríguez-Carvajal, Recent Developments of the Program FULLPROF, Commission on Powder Diffraction, 26, IUCr Newsl., 2001, pp. 12–19.
[43] J. Rodríguez-Carvajal, T. Roisnel, Line broadening analysis using FullProf*: determination of microstructural properties, Mater. Sci. Forum 443–444 (2004) 123–126.
[44] B. Wunderlich, Thermal Analysis of Polymeric Materials, Springer-Verlag, Berlin Heidelberg, 2005.
[45] L. Fontana, D.Q. Vinh, M. Santoro, S. Scandolo, F.A. Gorelli, R. Bini, M. Hanfland, High-pressure crystalline polyethylene studied by X-ray diffraction and *ab initio* simulations, Phys. Rev. B 75 (2007) 174112.
[46] S.H. Hyon, H. Taniuchi, R. Kitamaru, The orientation of crystal planes in polyethylene crystallized under compression, Bull. Inst. Chem. Res. Kyoto Univ. 51 (1973) 91–103.
[47] H. Ghasemi, N. Thoppey, X. Huang, J. Loomis, X. Li, J. Tong, J. Wang, G. Chen, High thermal conductivity ultra-high molecular weight polyethylene (UHMWPE) films. Fourteenth Intersociety Conference on Thermal and Thermomechanical Phenomena in Electronic Systems (ITherm), 2014, pp. 235–239.
[48] K.C. Cole, A. Ajji, in: I.M. Ward, P.D. Coates, M.M. Dumoulin (Eds.), Solid Phase Processing of Polymers, Carl Hanser Verlag, Munich, 2000, p. 33.
[49] J.L. White, in: Properties and Behaviour of Polymers, Wiley, Hoboken NJ, 2011, p. 883.
[50] Q. Chen, Z. Wang, S. Zhang, Y. Cao, J. Chen, Structure evolution and deformation behavior of polyethylene film during biaxial stretching, ACS Omega 5 (2020) 655–666.
[51] S. Krimm, Infrared dichroism in the 13.8μ band of nC36H74 single crystals and polyethylene, J. Chem. Phys. 22 (1954) 567–568.
[52] A. Keller, I. Sandeman, Investigation of unusual orientation in polyethylene by infrared spectroscopy, J. Polym. Sci. 15 (1955) 133–150.
[53] Y.V. Kissin, Infrared method for measuring orientation in polyethylene films, J. Polym. Sci. B 30 (1992) 1165–1172.
[54] R.G. Snyder, Vibrational spectra of crystalline n-paraffins. II. Intermolecular effects, J. Mol. Spectrosc. 7 (1961) 116–144.
[55] H. Hagemann, R.G. Snyder, A.J. Peacock, L. Mandelkern, Quantitative infrared methods for the measurement of crystallinity and its temperature dependence: polyethylene, Macromolecules 22 (1989) 3600–3606.
[56] P.J. Miller, J.F. Jackson, R.S. Porter, Infrared dichroism of polyethylene crystallized by orientation and pressure in a capillary viscometer, J. Polym. Sci. B 11 (1973) 2001–2012.
[57] J.R. Nielsen, R.F. Holland, Dichroism and interpretation of the infrared bands of oriented crystalline polyethylene, J Mol Spectro 6 (1961) 394–418.
[58] M.H. Klopffer, B. Flaconnèche, Transport properties of gases in polymers: bibliographic review, Oil Gas Sci. Technol. 56 (2001) 223–244.
[59] P. DeLassus, in: Kirk-Othmer Encyclopedia of Chemical Technology, fourth ed., Volume 3, Wiley, New York, 2001, p. 486.
[60] S.C. George, S. Thomas, Transport phenomena through polymeric systems, Prog. Polym. Sci. 26 (2001) 985–1017.
[61] T. Naylor, in: C. Booth, C. Price (Eds.), Comprehensive Polymer Science and Supplements, ume 2, Elsevier, Oxford, 1996, p. 643.
[62] A.S. Michaels, R.B. Parker Jr, Sorption and flow of gases in polyethylene, J. Polym. Sci. 41 (1959) 53–71.
[63] H. Sha, I.R. Harrison, CO_2 permeability and amorphous fractional free-volume in uniaxially drawn HDPE, J. Polym. Sci. B 30 (1992) 915–922.
[64] J.P. Paulos, E.L. Thomas, Effect of postdrawing on the permeability of gases in blown polyethylene film, J. Appl. Polym. Sci. 25 (1980) 15–23.
[65] P.S. Holden, G.A.J. Orchard, I.M. Ward, A study of the gas barrier properties of highly oriented polyethylene, J Polym Sci Pol Phys 23 (1985) 709–731.
[66] D.R. Breese, G. Beaucage, Effect of machine direction orientation (MDO) on the moisture and oxygen barrier properties of HMW-PE films. TAPPI Conference Papers, 2005.
[67] B. Fayolle, E. Richaud, X. Colin, J. Verdu, Review: degradation-induced embrittlement in semi-crystalline polymers having their amorphous phase in rubbery state, J. Mater. Sci. 43 (2008) 6999–7012.
[68] R. Greenwood, N. Weir, Effects of photo-degradation on the permeability and diffusivity characteristics of poly(*p*-methylstyrene), Makromol. Chem. 176 (1975) 2041–2051.
[69] J.-L. Philippart, J.-L. Gardette, Analyse du Photovieillissement des Matériaux Polymères par Evolution de la Perméabilité aux Gaz, Makromol. Chem. 187 (1986) 1639–1650.
[70] S. Nakatsuka, A. Andrady, Studies studies on enhanced degradable plastics. HI. The effect of weathering of polyethylene and (Ethylene-Carbon monoxide) copolymers on moisture and carbon dioxide permeability, J. Environ. Polym. Degrad. 2 (1994) 161–167.
[71] X. Ye, H. Pi, S. Guo, A novel route for preparation of PVC sheets with high UV irradiation resistance, J. Appl. Polym. Sci. 117 (2010) 2899–2906.
[72] J.-L. Gardette, A. Colin, S. Trivis, S. German, S. Therias, Impact of photooxidative degradation on the oxygen permeability of poly(ethyleneterephthalate), Polym Degrad Stab 103 (2014) 35–41.
[73] S. Collin, P.-O. Bussière, J.-L. Gardette, J. Perdereau, R. Gorjup, S. Therias, Accelerated photo-aging of organic coatings used as protective layersfor Blu-ray Discs, Prog Org Coat 84 (2015) 9–17.
[74] P. Scarfato, D. Acierno, P. Russo, Photooxidative weathering of biodegradable nanocomposite films containing halloysite, Polym Comp 2015 (2015) 1169–1175.
[75] V. Siracusa, N. Lotti, A. Munari, Rosa M. Dalla, Poly(butylene succinate) and poly (butylene succinate-co-adipate) for food packaging applications: gas barrier properties after stressed treatments, Polym Degrad Stab 119 (2015) 35–45.
[76] M. Gigli, L. Genovese, N. Lotti, Dalla Munari, M. Rosa, V. Siracusa, Gas barrier and thermal behavior of long chain aliphatic polyesters after stressed treatments, Polym. Plast. Technol. Eng. 56 (2017) 71–82.